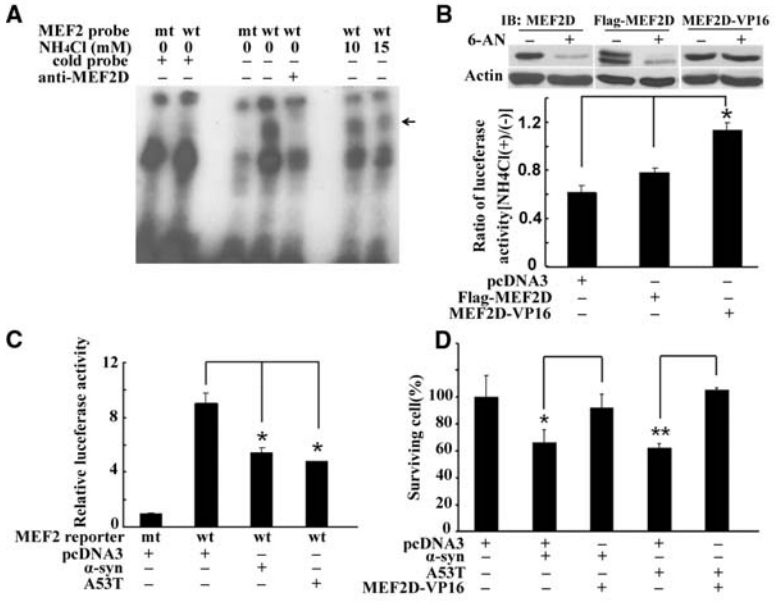

Fig. 4. Impairment of MEF2 function and neuronal survival after blockade of CMA. (**A**) Inhibition of MEF2D DNA binding activity by NH_4Cl. MEF2D DNA binding activity in SN4741 cells was assessed by EMSA after NH_4Cl treatment (arrow indicates the specific MEF2D-probe complex). (**B**) Effect of enhanced nuclear MEF2D on NH_4Cl-mediated inhibition. Levels of endogenous and transfected MEF2D in the nucleus (top panel) and MEF2 reporter activities (lower graph) in SN4741 cells were determined after 6-AN or NH_4Cl treatment, respectively ($n = 3$, $^*P < 0.05$). (**C**) Inhibition of MEF2 transactivation activity by α-synuclein. MEF2 reporter gene expression was measured after 36 hours of overexpression of wild-type or A53T α-synuclein in SN4741 cells ($n = 4$, $^*P < 0.05$). (**D**) Effect of increasing nuclear MEF2D function on α-synuclein–induced neuronal death. The viability of SN4741 cells was determined by WST assay after overexpression of indicated proteins (mean ± SEM, $n = 4$; $^*P < 0.05$, $^{**}P < 0.01$).

in neuronal viability (Fig. 4D). Coexpression of MEF2D-VP16 protected the cells against α-synuclein toxicity.

Our studies link CMA directly to the nuclear survival machinery. Because only α-synuclein mutants block substrate uptake in CMA (*18*), it has been unclear why an increase in the level of wild-type α-synuclein causes PD (*23*). Our findings that α-synuclein disrupts CMA-mediated degradation of MEF2D at a step prior to substrate uptake explain the toxic effects of both wild-type and mutant α-synuclein. Expression of Hsc70 suppresses α-synuclein toxicity in a *Drosophila* model of PD (*24*), consistent with our finding that maintenance of MEF2 function attenuates α-synuclein–induced neuronal death. Blocking CMA is accompanied by a clear decline of MEF2 function. Because the accumulated MEF2D binds poorly to DNA, the finding that the accumulated MEF2D binds poorly to DNA suggests important mechanisms in addition to nuclear export for the control of MEF2 activity. MEF2s play diverse roles in non-neuronal systems under physiological and pathological conditions (*25*). Our findings raise the possibility that degradation of MEF2s by CMA may function in other processes.

References and Notes

1. Z. Mao, A. Bonni, F. Xia, M. Nadal-Vicens, M. E. Greenberg, *Science* **286**, 785 (1999).
2. X. Gong *et al.*, *Neuron* **38**, 33 (2003).
3. P. Gonzalez *et al.*, *Neurosci. Lett.* **411**, 47 (2007).
4. P. D. Smith *et al.*, *J. Neurosci.* **26**, 440 (2006).
5. X. Tang *et al.*, *J. Neurosci.* **25**, 4823 (2005).
6. J. F. Dice, *Autophagy* **3**, 295 (2007).
7. R. A. Nixon, *Trends Neurosci.* **29**, 528 (2006).
8. D. C. Rubinsztein, *Nature* **443**, 780 (2006).
9. U. Bandhyopadhyay, A. M. Cuervo, *Exp. Gerontol.* **42**, 120 (2007).
10. J. H. Son *et al.*, *J. Neurosci.* **19**, 10 (1999).
11. P. Saftig *et al.*, *EMBO J.* **14**, 3599 (1995).
12. H. S. Chun *et al.*, *J. Neurochem.* **76**, 1010 (2001).
13. A. M. Cuervo, E. Knecht, S. R. Terlecky, J. F. Dice, *Am. J. Physiol.* **269**, C1200 (1995).
14. A. Massey, R. Kiffin, A. M. Cuervo, *Int. J. Biochem. Cell Biol.* **36**, 2420 (2004).
15. P. F. Finn, N. T. Mesires, M. Vine, J. F. Dice, *Autophagy* **1**, 141 (2005).
16. P. O. Seglen, P. B. Gordon, *Proc. Natl. Acad. Sci. U.S.A.* **79**, 1889 (1982).
17. A. E. Majeski, J. F. Dice, *Int. J. Biochem. Cell Biol.* **36**, 2435 (2004).
18. A. M. Cuervo, L. Stefanis, R. Fredenburg, P. T. Lansbury, D. Sulzer, *Science* **305**, 1292 (2004).
19. J. L. Webb, B. Ravikumar, J. Atkins, J. N. Skepper, D. C. Rubinsztein, *J. Biol. Chem.* **278**, 25009 (2003).
20. L. J. Martin *et al.*, *J. Neurosci.* **26**, 41 (2006).
21. Z. Mao, M. Wiedmann, *J. Biol. Chem.* **274**, 31102 (1999).
22. H. P. Bogerd, R. A. Fridell, R. E. Benson, J. Hua, B. R. Cullen, *Mol. Cell. Biol.* **16**, 4207 (1996).
23. A. B. Singleton *et al.*, *Science* **302**, 841 (2003).
24. P. K. Auluck, H. Y. E. Chan, J. Q. Trojanowski, V. M.-Y. Lee, N. M. Bonini, *Science* **295**, 865 (2002); published online 20 December 2001 (10.1126/science.1067389).
25. M. P. Czubryt, E. N. Olson, *Recent Prog. Horm. Res.* **59**, 105 (2004).

26. We thank H. Rees and D. Cooper at Emory Neuroscience NINDS Core Facility (NS055077) and UAB Neuroscience Core Facility (NS47466 and NS57098) for assistance in imaging and immunohistochemistry analysis, and J. Blum and A. M. Cuervo for Hsc70 and Lamp2a constructs. Supported by NIH grants NS048254 (Z.M.), AG023695 (Z.M.), and NS038065 (M.L.) and by Emory and UAB Alzheimer's Disease Research Center pilot grants (Z.M. and J.J.S.) and the Robert Woodruff Health Sciences Center Fund (Z.M.).

Supporting Online Material

www.sciencemag.org/cgi/content/full/323/5910/124/DC1
Materials and Methods
Figs. S1 to S9
References

18 September 2008; accepted 5 November 2008
10.1126/science.1166088

Signal Sequences Activate the Catalytic Switch of SRP RNA

Niels Bradshaw,* Saskia B. Neher,* David S. Booth, Peter Walter†

The signal recognition particle (SRP) recognizes polypeptide chains bearing a signal sequence as they emerge from the ribosome, and then binds its membrane-associated receptor (SR), thereby delivering the ribosome–nascent chain complex to the endoplasmic reticulum in eukaryotic cells and the plasma membrane in prokaryotic cells. SRP RNA catalytically accelerates the interaction of SRP and SR, which stimulates their guanosine triphosphatase (GTPase) activities, leading to dissociation of the complex. We found that although the catalytic activity of SRP RNA appeared to be constitutive, SRP RNA accelerated complex formation only when SRP was bound to a signal sequence. This crucial control step was obscured because a detergent commonly included in the reaction buffer acted as a signal peptide mimic. Thus, SRP RNA is a molecular switch that renders the SRP-SR GTPase engine responsive to signal peptide recruitment, coupling GTP hydrolysis to productive protein targeting.

Secretory and transmembrane proteins are delivered to the membrane cotranslationally by the signal recognition particle (SRP) and its membrane-associated receptor (SR) (*1*). SRP recognizes signal sequences as they emerge from the ribosome (*2*) and then associates with SR at the membrane where the ribosome is transferred to the translocon. The guanosine triphos-

phatase (GTPase) domains of SRP and SR mediate this interaction cycle (*3*). Interaction of SRP with SR leads to the reciprocal stimulation of their GTPase activities, and GTP hydrolysis dissociates the complex (*4*, *5*). In *Escherichia coli*, SR is a single protein, FtsY, and SRP consists of 4.5*S* RNA and a single protein, Ffh (*6*). 4.5*S* RNA catalyzes the interaction of Ffh and FtsY, accelerating both on and off rates by a factor of more than 100 (*7*).

If the energy of GTP hydrolysis is to be harnessed for protein targeting, recruitment of targeting substrates by SRP should be coupled to the SRP-SR interaction cycle. Both signal sequences and 4.5*S* RNA bind to the M domain of Ffh, which suggests that the catalytic activity of 4.5*S* RNA could be responsive to signal sequence binding (*8*). However, under typical assay conditions, 4.5*S* RNA is constitutively active, negating this role for the RNA (*4*, *7*, *9*, *10*). A small amount of the nonionic detergent octaethyleneglycol dodecylether ($C_{12}E_8$) has been used in assays for SRP function, including kinetic characterization of the Ffh-FtsY interaction (*4*, *7*, *9*–*11*). We found that $C_{12}E_8$ was required for the stimulation of Ffh-FtsY binding rate caused by 4.5*S* RNA (Fig. 1A and table S1).

Assembly of the Ffh-FtsY complex can be measured by tryptophan fluorescence (*7*, *9*). In the presence of 4.5*S* RNA, $C_{12}E_8$ stimulated the rate of Ffh-FtsY association by a factor of 70 (Fig. 1A). Likewise, the stimulation of Ffh-FtsY disassembly caused by 4.5*S* RNA required $C_{12}E_8$ (faster with $C_{12}E_8$ than without by a factor of 23; Fig. 1B and table S1). $C_{12}E_8$ had no effect on the assembly or disassembly reactions in the absence of 4.5*S* RNA (Fig. 1, A and B). Thus, $C_{12}E_8$ is not a passive stabilizing additive but "activates" 4.5*S* RNA to accelerate Ffh-FtsY complex formation. Moreover, as most previous studies characterizing 4.5*S* RNA catalysis of the Ffh-FtsY interaction were carried out with detergent, they monitored this activated state.

The molecular properties of $C_{12}E_8$ that are important for activating 4.5*S* RNA suggested that it acts as a signal peptide mimic. We tested E_8, the nonionic head group of $C_{12}E_8$, and the detergents cetyltrimethylammonium bromide (CTABr) and sodium dodecyl sulfate (SDS), which share a long carbon chain with $C_{12}E_8$ but are positively and negatively charged, respectively (Fig. 1, C and D). CTABr stimulated binding similarly to $C_{12}E_8$, whereas SDS and E_8 did not (Fig. 1D). Thus, the long carbon chain of $C_{12}E_8$ with a neutral or positively charged head group is sufficient to activate 4.5*S* RNA. This suggests that $C_{12}E_8$ acts as a signal peptide mimic, because signal peptides generally have a hydrophobic core and positively but not negatively charged amino acids (*12*). Additionally, Ffh was crystallized with detergents (*13*), and density in the signal sequence–binding groove may have been attributable to the detergent. Finally, the Hill coefficient (n = 5.8) for $C_{12}E_8$ stimulation of Ffh–4.5*S* RNA–FtsY complex formation (fig. S1A) suggested that at least six detergent molecules cooperate to activate each Ffh–4.5*S* RNA and corresponded well with the size of the putative signal sequence–binding pocket in Ffh (fig. S1B).

We sought to determine whether signal peptides activate 4.5*S* RNA in the absence of $C_{12}E_8$. Because most signal peptides are insoluble (*14*), we chose the ΔEspP signal peptide (*15*), which is less hydrophobic than most signal peptides. We measured binding of ΔEspP peptide labeled with carboxyfluorescein (ΔEspP-FAM) to Ffh by fluorescence anisotropy. ΔEspP-FAM bound Ffh–4.5*S* RNA with an equilibrium dissociation constant (K_d) of 1.5 ± 0.4 μM (Fig. 2A). The K_d for Ffh alone was 19.6 ± 6.4 μM (Fig. 2A), which confirms that 4.5*S* RNA contributes to the binding of signal peptides as predicted (*8*). The addition of $C_{12}E_8$ weakened ΔEspP-FAM binding to Ffh–4.5*S* RNA (K_d = 5.5 ± 1.5 μM) but not to Ffh alone (21.6 ± 7.9 μM) (Fig. 2B), suggesting that ΔEspP and detergent compete for binding to SRP. ΔEspP-FAM did not bind Ffh lacking its signal sequence–binding M domain (Fig. 2A), binding was reversible (fig. S2A), and ΔEspP-FAM did not impair the solubility of Ffh–4.5*S* RNA (fig. S2, B and C).

To test whether saturating concentrations of ΔEspP stimulate the activity of 4.5*S* RNA, we used ΔEspP with added lysines at the C terminus to improve its solubility [ΔEspP* (*16*)]. Like $C_{12}E_8$, ΔEspP* accelerated Ffh–4.5*S* RNA–FtsY association (by a factor of >40; Fig. 2C and table S1) and dissociation (by a factor of ~10; table S1) but had no effect in the absence of 4.5*S* RNA (Fig. 2C and table S1). In the presence of both $C_{12}E_8$ and ΔEspP*, the rate of Ffh–4.5*S* RNA–FtsY complex formation was not substantially changed relative to individual additions (table

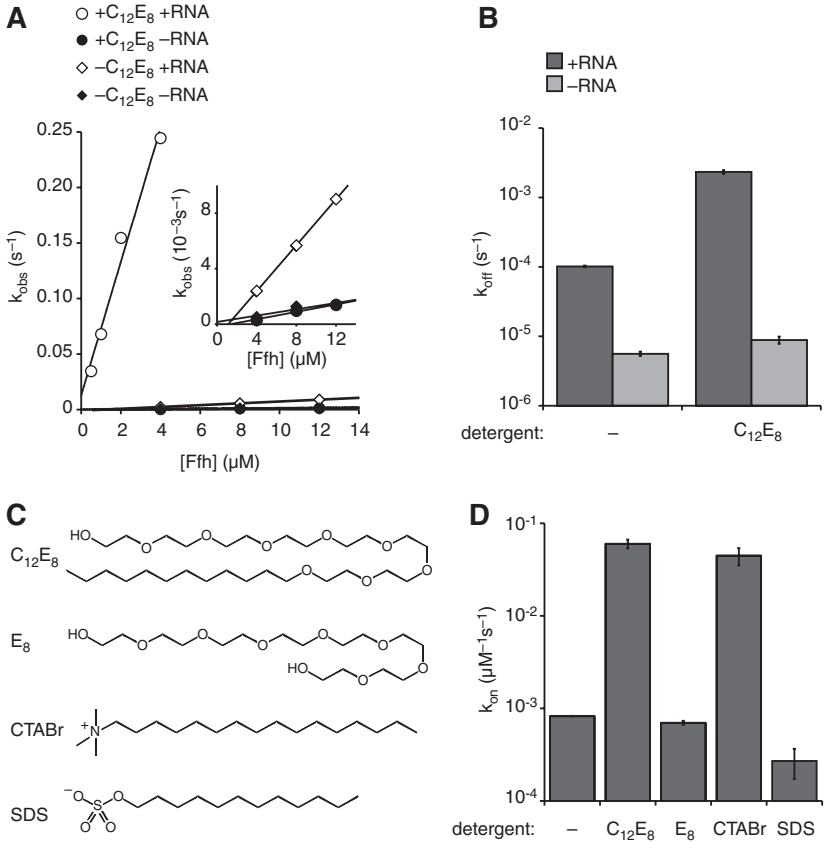

Fig. 1. Detergent activates 4.5*S* RNA to catalyze the Ffh-FtsY interaction. (**A**) $C_{12}E_8$ stimulates the binding of Ffh and FtsY only in the presence of 4.5*S* RNA. Observed binding rates for formation of Ffh-FtsY complexes are plotted as a function of Ffh concentration, [Ffh], in the presence and absence of 4.5*S* RNA and 185 μM $C_{12}E_8$. Lines represent fits to the equation $k_{obs} = k_{off} + k_{on}$[Ffh]. Inset shows the slow reactions on an expanded scale. (**B**) $C_{12}E_8$ activates 4.5*S* RNA stimulation of Ffh-FtsY complex dissociation. Dissociation rate constants are plotted in the absence and presence of $C_{12}E_8$. (**C**) Chemical structures of $C_{12}E_8$, E_8, CTABr, and SDS. (**D**) Association rate constants for Ffh–4.5*S* RNA–FtsY complex formation with no detergent, 185 μM $C_{12}E_8$, 100 μM E_8, 70 μM CTABr, or 100 μM SDS. Error bars in (B) and (D) are SEs of the fits.

Howard Hughes Medical Institute, 4000 Jones Bridge Road, Chevy Chase, MD 20815, USA, and Department of Biochemistry and Biophysics, University of California, Genentech Hall, MC 2200, 600 16th Street, San Francisco, CA 94158, USA.

*These authors contributed equally to this work.
†To whom correspondence should be addressed. E-mail: pwalter@biochem.ucsf.edu

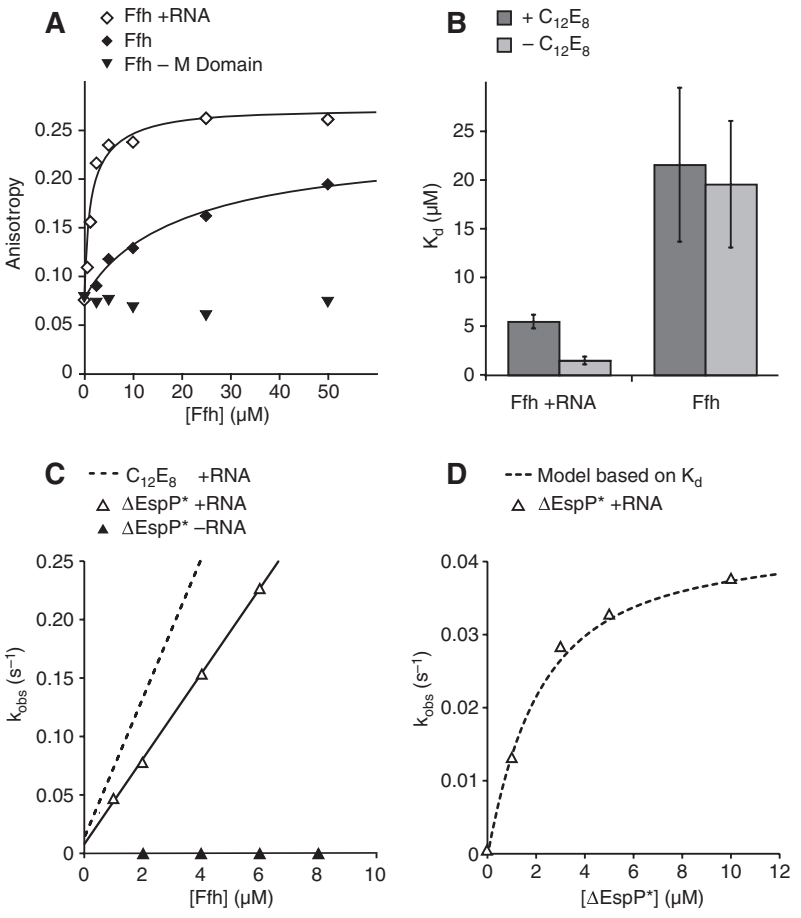

Fig. 2. ΔEspP binds SRP with micromolar affinity and stimulates 4.5*S* RNA catalysis of Ffh-FtsY interaction. (**A**) Fluorescence anisotropy of ΔEspP-FAM is plotted as a function of [Ffh]. Lines represent fits to the equation Anisotropy = $\text{Anisotropy}_{\text{free}}$ + $\text{Anisotropy}_{\text{bound}}$([Ffh]/($K_d$ + [Ffh])). (**B**) $C_{12}E_8$ increased the K_d of ΔEspP for Ffh–4.5*S* RNA. K_d values for ΔEspP binding to Ffh from fluorescence anisotropy in the presence and absence of 4.5*S* RNA are plotted. Dark bars represent K_d in the presence of 185 μM $C_{12}E_8$. Error bars are SEs of the fits. (**C**) In the presence of 4.5*S* RNA, ΔEspP stimulates the association rate for Ffh-FtsY complex formation. Observed rate constants are plotted as a function of [Ffh]. Lines are fits to the equation $k_{obs} = k_{off} + k_{on}$[Ffh]. The dashed line is a reference to the binding rate in the presence of $C_{12}E_8$ from Fig. 1. (**D**) ΔEspP* activates 4.5*S* RNA by binding to SRP. Observed rates for 1 μM Ffh–4.5*S* RNA binding to 1 μM FtsY are plotted as a function of ΔEspP* concentration. The dashed line represents the equation k_{obs} = [(fraction bound)(maximum stimulated rate)] + [(fraction unbound)(unstimulated rate)], where the fraction bound was calculated from the K_d measured in (A); $\chi^2 = 5.4 \times 10^{-6}$.

S1). Thus, the ΔEspP peptide and $C_{12}E_8$ act by the same mechanism.

If ΔEspP* activates 4.5*S* RNA by associating with SRP, then the rate of Ffh–4.5*S* RNA–FtsY interaction should correlate with the fraction of ΔEspP*-bound SRP (calculated from the K_d in Fig. 2A). We measured the rate of Ffh–4.5*S* RNA and FtsY interaction as a function of ΔEspP* concentration (Fig. 2D). When we compared the observed Ffh-FtsY binding rates to the rate predicted from the fraction of SRP bound to ΔEspP* (Fig. 2A), the data matched this model exceptionally well (Fig. 2D).

In addition to accelerating Ffh-FtsY association, 4.5*S* RNA increases the rate of GTP hydrolysis by Ffh^{GTP}-FtsY^{GTP} complexes (*4*) (fig. S3). However, neither ΔEspP* nor $C_{12}E_8$ affected this rate (fig. S3). Thus, signal peptides specifically affect the ability of 4.5*S* RNA to accelerate Ffh-FtsY complex formation.

To assess the specificity of 4.5*S* RNA activation, we used a version of ΔEspP* bearing $\text{Phe}^{12} \rightarrow$ Ala and $\text{Leu}^{15} \rightarrow$ Thr mutations [ΔEspP(F12A, L15T)*] that reduce SRP-dependent targeting in vivo (*15*). In the presence of 10 μM ΔEspP(F12A, L15T)*, the 4.5*S* RNA–stimulated association and dissociation of Ffh and FtsY was slower than that measured with "wild-type" ΔEspP* by a factor of ~5 (Fig. 3A and table S1). Similar to ΔEspP*, ΔEspP (F12A, L15T)* had no effect in the absence of 4.5*S* RNA (Fig. 3A). To determine whether this was due to reduced binding of ΔEspP(F12A, L15T)* to SRP, we measured the K_d by fluorescence anisotropy and found that binding was substantially weaker (K_d = 87 ± 18 μM, Fig. 3B). Consistent with this result, increasing concentrations of ΔEspP(F12A, L15T)* increased the observed rate for SRP-FtsY association (fig. S4).

Thus, SRP RNA acts as a switchable regulatory module at the center of the SRP protein-targeting machine to link recruitment of cargo (a signal peptide) to the next step in the targeting reaction (binding to SR). If free SRP and SR interacted efficiently with each other, they would undergo futile cycles of binding and GTP hydrolysis. Cargo-dependent activation of SRP RNA

Fig. 3. Mutations in ΔEspP that impair SRP-mediated targeting show decreased binding to SRP and decreased stimulation of 4.5*S* RNA. (**A**) ΔEspP(F12A, L15T)* stimulates SRP-FtsY complex formation less than does ΔEspP*. The dashed line represents the ΔEspP* + RNA peptide binding rate from Fig. 2C. (**B**) Fluorescence anisotropy of FAM-labeled ΔEspP bearing $\text{Phe}^{12} \rightarrow$ Ala and $\text{Leu}^{15} \rightarrow$ Thr mutations [ΔEspP(F12A, L15T)] is plotted as a function of [Ffh +RNA]. Line is fit as in Fig. 2A.

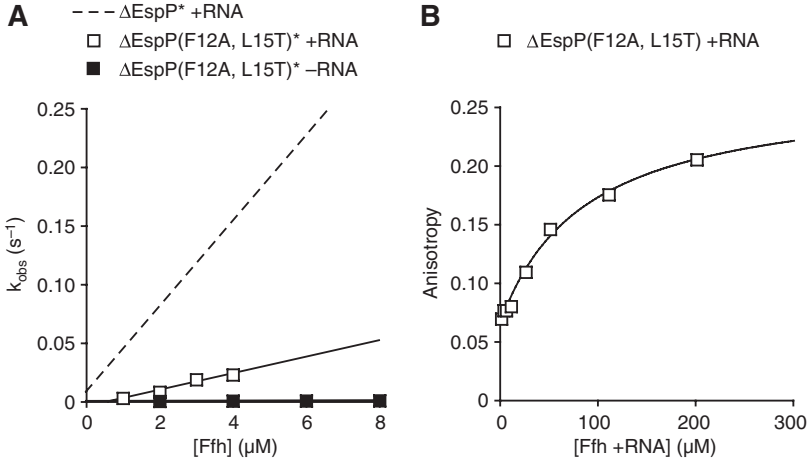

prevents this, harnessing the energy of GTP hydrolysis for protein targeting.

High-affinity interaction of SRP with ribosomes can occur before SRP interaction with the signal peptide when a short nascent chain is still inside the ribosome, raising the question of how SRP selectively targets signal sequence–containing substrates (*17*). Our results show that the interaction of the signal peptide with SRP accelerates SRP-SR complex formation, thereby providing a mechanism for selective delivery of appropriate substrates to the membrane. This is conceptually analogous to the kinetic mechanism by which translation achieves fidelity, where cognate codon-anticodon pairing accelerates GTP hydrolysis by elongation factor Tu (EF-Tu) (*18*, *19*).

Our results provide an intuitive model for how each step of the targeting process activates the next to achieve productive, directional targeting. Signal peptides bind to SRP's conformationally flexible M domain that forms a continuous surface with SRP RNA (*8*, *13*). Binding induces a conformational change that activates SRP RNA (*20*). Activated SRP RNA facilitates the displacement of the N-terminal helices of SRP and SR that slow their association without SRP RNA (*21*). This commits the ribosome–nascent chain complex to membrane targeting. The kinetic control described here, where substrate recruitment accelerates downstream interactions, provides a generalizable principle for coordination of multistep pathways.

References and Notes

1. R. J. Keenan, D. M. Freymann, R. M. Stroud, P. Walter, *Annu. Rev. Biochem.* **70**, 755 (2001).
2. D. Zopf, H. D. Bernstein, A. E. Johnson, P. Walter, *EMBO J.* **9**, 4511 (1990).
3. J. D. Miller, H. Wilhelm, L. Gierasch, R. Gilmore, P. Walter, *Nature* **366**, 351 (1993).
4. P. Peluso, S. O. Shan, S. Nock, D. Herschlag, P. Walter, *Biochemistry* **40**, 15224 (2001).
5. T. Powers, P. Walter, *Science* **269**, 1422 (1995).
6. M. A. Poritz *et al.*, *Science* **250**, 1111 (1990).
7. P. Peluso *et al.*, *Science* **288**, 1640 (2000).
8. R. T. Batey, R. P. Rambo, L. Lucast, B. Rha, J. A. Doudna, *Science* **287**, 1232 (2000).
9. J. R. Jagath, M. V. Rodnina, W. Wintermeyer, *J. Mol. Biol.* **295**, 745 (2000).
10. X. Zhang, S. Kung, S. O. Shan, *J. Mol. Biol.* **381**, 581 (2008).
11. P. Walter, G. Blobel, *Proc. Natl. Acad. Sci. U.S.A.* **77**, 7112 (1980).
12. G. von Heijne, *J. Mol. Biol.* **184**, 99 (1985).
13. R. J. Keenan, D. M. Freymann, P. Walter, R. M. Stroud, *Cell* **94**, 181 (1998).
14. J. F. Swain, L. M. Gierasch, *J. Biol. Chem.* **276**, 12222 (2001).
15. J. H. Peterson, C. A. Woolhead, H. D. Bernstein, *J. Biol. Chem.* **278**, 46155 (2003).
16. See supporting material on *Science* Online.
17. T. Bornemann, J. Jockel, M. V. Rodnina, W. Wintermeyer, *Nat. Struct. Mol. Biol.* **15**, 494 (2008).
18. T. Pape, W. Wintermeyer, M. Rodnina, *EMBO J.* **18**, 3800 (1999).
19. J. M. Ogle, V. Ramakrishnan, *Annu. Rev. Biochem.* **74**, 129 (2005).
20. N. Bradshaw, P. Walter, *Mol. Biol. Cell* **18**, 2728 (2007).
21. S. B. Neher, N. Bradshaw, S. N. Floor, J. D. Gross, P. Walter, *Nat. Struct. Mol. Biol.* **15**, 916 (2008).

22. We thank J. Weissman, C. Gross, P. Egea, C. Gallagher, A. Korennykh, A. Acevedo, W. Weare, and J. Kardon for assistance and comments. Supported by NIH grant ROI GM32384 (P.W.), an NSF predoctoral fellowship (N.B.), the Jane Coffin Childs Memorial Fund (S.B.N.), and National Institute of General Medical Sciences fellowship R25 GM56847 (D.S.B.). P.W. is an Investigator of the Howard Hughes Medical Institute.

Supporting Online Material

www.sciencemag.org/cgi/content/full/323/5910/127/DC1
Materials and Methods
Figs. S1 to S5
Table S1
References

16 September 2008; accepted 5 November 2008
10.1126/science.1165971

Floral Iridescence, Produced by Diffractive Optics, Acts As a Cue for Animal Pollinators

Heather M. Whitney,[1]* Mathias Kolle,[2,3]* Piers Andrew,[3] Lars Chittka,[4] Ullrich Steiner,[2,3]† Beverley J. Glover[1]†

Iridescence, the change in hue of a surface with varying observation angles, is used by insects, birds, fish, and reptiles for species recognition and mate selection. We identified iridescence in flowers of *Hibiscus trionum* and *Tulipa* species and demonstrated that iridescence is generated through diffraction gratings that might be widespread among flowering plants. Although iridescence might be expected to increase attractiveness, it might also compromise target identification because the object's appearance will vary depending on the viewer's perspective. We found that bumblebees (*Bombus terrestris*) learn to disentangle flower iridescence from color and correctly identify iridescent flowers despite their continuously changing appearance. This ability is retained in the absence of cues from polarized light or ultraviolet reflectance associated with diffraction gratings.

Biological iridescence results from various mechanisms, including multilayered materials, crystalline inclusions, and surface diffraction gratings (*1*–*6*). Diffraction gratings, surface striations of particular amplitude and frequency, cause interference, giving rise to an angular color variation (*7*). Although epidermal plant cell shape has been shown to influence the capture of all wavelengths of light by pigments (*8*–*10*), the mechanisms of iridescence have been poorly studied in plants; however, multilayered effects are occasionally observed in leaves (*11*, *12*).

Hibiscus trionum petals are white with a patch of red pigment at the base. This pigmented patch is iridescent, appearing blue, green, and yellow depending on the angle from which it is viewed (Fig. 1, A and B). Scanning electron microscopy (SEM) shows a sharply defined difference between the surface structure overlying the pigment and the rest of the petal (Fig. 1C). This iridescence is visible to the human eye; however, in flowers with similar surface structures, such as many species of *Tulipa* (table S1), the iridescence is only evident to humans when the pigment color and petal surface structure are separated.

When the surface structure of hibiscus and tulip petals was replicated in colorless optical epoxy (*13*), iridescent color was visible independent of pigment (fig. S3A). SEM of these replicas showed that long, ordered, cuticular striations overlay the iridescent epidermal cells. These cuticular striations resemble a diffraction grating. The diffraction grating of compact discs (CDs) has been previously characterized (*7*), so we used SEM to compare an epoxy cast made from the plastic interior of a disassembled CD with a cast of *Tulipa kolpakowskiana* (Fig. 2, A and B). The tulip cast (Fig. 2, C and D) shows a rounded cross-section of the striations (as opposed to the square profile of the CD) and a long wavelength undulation with a periodicity of 29 ± 2 μm, reflecting the surface of the epidermal cells.

We further investigated the tulip casts with optical spectroscopy in the 300-to-900-nm wavelength range [near-ultraviolet (near-UV) to infrared]. A collimated light beam of ~2 mm in diameter was reflected off the cast at an incidence angle $\theta_I = 30°$, and the reflected and scattered light was detected at angles θ_D varying from 0° to 90° in 1° steps (fig. S1). The angular detection aperture was less than 1° [supporting online material (SOM) text].

The spectrally resolved reflectivity was determined for the tulip cast (Fig. 3, A and B),

[1]Department of Plant Sciences, University of Cambridge, Downing Street, Cambridge CB2 3EA, UK. [2]Department of Physics, Cavendish Laboratory, University of Cambridge, J. J. Thomson Avenue, Cambridge CB3 0HE, UK. [3]Nanoscience Centre, University of Cambridge, 11 J. J. Thomson Avenue, Cambridge, CB3 0FF, UK. [4]School of Biological and Chemical Sciences, Queen Mary University of London, London E1 4NS, UK.

*These authors contributed equally to this work.
†To whom correspondence should be addressed. E-mail: u.steiner@phy.cam.ac.uk (U.S.); bjg26@cam.ac.uk (B.J.G.)

Supporting Online Material.

Materials and Methods

Reagents. Full length untagged *E. coli* Ffh, 6-his tagged *E. coli* FtsY (amino acids 47-497), and *E. coli* 4.5S RNA were purified as previously described(*1*). As previously, Ffh was purified in the absence of detergents. Synthetic signal peptides were ordered from Elim Biosciences (unlabeled) or Anaspec (FAM labeled). All peptides were purified to >80% purity and the molecular mass of the peptides were confirmed by mass spectrometry. In all cases, a single peak was present at the predicted mass. Peptides for kinetic assays, denoted by an *, were used at higher concentrations and therefore contain four additional lysines appended at the C-terminus to enhance solubility and a C-terminal phenylalanine converted to tryptophan to facilitate concentration measurements. Peptides used in this study are; ΔEspP* (MKK HKR ILA LCF LGL LQS SYS WAK KKK), ΔEspP(F12A, L15T)* (MKK HKR ILA LCA LGT LQS SYS WAK KKK), ΔEspP-FAM (MKK HKR ILA LCF LGL LQS SYS FA K(5-FAM)-NH2), and ΔEspP(F12A, L15T)-FAM (MKK HKR ILA LCA LGT LQS SYS FA K(5-FAM)-NH2).

Ffh/FtsY binding assays. Fluorescence assays monitoring the association of Ffh and FtsY were performed as described(*1*). Assays were performed at 23°C in 50mM Hepes pH7.5, 150mM KOAc, 2mM $Mg(OAc)_2$, 2mM DTT and 100μM GppNHp. Data were collected on a stopped-flow fluorimeter (KinTek) for fast reactions or a SLM 8100 for slow reactions with an excitation wavelength of 290 nm and an emission wavelength of 340 nm.

Observed binding rates were calculated by fitting the fluorescence data to a single exponential equation. To determine association rate constants, observed binding rates were plotted as a function of [Ffh] and fit to the equation $k_{obs}=k_{on}[Ffh]+k_{off}$. For experiments with ΔEspP peptide, Ffh, FtsY and ΔEspP were mixed and binding was initiated by the addition of GppNHp. Peptides were always used at 10μM concentration unless otherwise noted.

To ensure that the increase in tryptophan fluorescence observed in the presence of ΔEspP* was caused by the specific interaction of Ffh and FtsY rather than by nonspecific aggregation induced by the peptide, reactions were performed by premixing Ffh, 4.5SRNA, FtsY, and ΔEspP*, and initiating the reaction by adding GppNHp. Additionally, pelleting assays (**Fig. S2C**) and gel filtration (data not shown) confirmed that the peptide did not induce aggregation of the proteins.

Dissociation rate constants were determined by forming complexes with 4μM of each protein and then mixing with an equal volume of 4mM GDP•Mg^{2+}. The fluorescence data was then fit to a single exponential equation corrected for photobleaching to determine the k_{off}.

Peptide-Ffh binding assays. Fluorescence anisotropy was measured on a ISS K2 fluorimeter in 50mM Hepes pH7.5, 150mM KOAc, 2mM $Mg(OAc)_2$, 2mM DTT with or without 185 μM $C_{12}E_8$ as noted in the text. FAM-labeled peptides (0.5 μM) were

combined with varying concentrations of Ffh or Ffh-4.5S RNA and allowed to equilabrate for at least 10 minutes at room temperature. Samples were excited at 492 nm and measured at 520 nm. Each reading was taken for 30 seconds, averaged and corrected against a minus peptide sample for light scattering.

Figures and Legends

Figure S1. A. Concentration dependence of $C_{12}E_8$ activation of 4.5S RNA. Observed binding rates were determined for reactions with 1μM Ffh, 0.1μM FtsY, and 1.5μM 4.5SRNA as a function of $C_{12}E_8$ concentration. Data were fit to the equation $k_{obs}=[C_{12}E_8]^n/([C_{12}E_8]^n+K_{1/2}{}^n)$ giving $K_{1/2}$=60±0.7μM and n=5.8±0.4μM. Half-maximal stimulation (60μM) was achieved below the critical micelle concentration of C12E8 (90 μM(*2*)), suggesting that free detergent molecules activate 4.5S RNA. This is also supported by the fact that CTABr activates 4.5S RNA at concentrations significantly below its CMC (approximately 1mM). **B.** $C_{12}E_8$ may act as a signal peptide mimic. Hypothetical model of $C_{12}E_8$ binding in the putative signal sequence binding groove of the M-domain of Ffh (PDB ID 2FFH)(*3*). In this crystal form of Ffh, M-domains from adjacent molecules in the crystal packing are twinned so that the hydrophobic groove of each M-domain is partially occupied by the other. Due to the size and hydrophobic nature of the groove it is assumed to be the signal peptide binding site. We therefore generated a molecular model of $C_{12}E_8$ in the groove using ChemDraw3D. Six $C_{12}E_8$ molecules were placed into the signal sequence binding pocket manually and the energy of the detergent was minimized by an MM2 minimization.

A

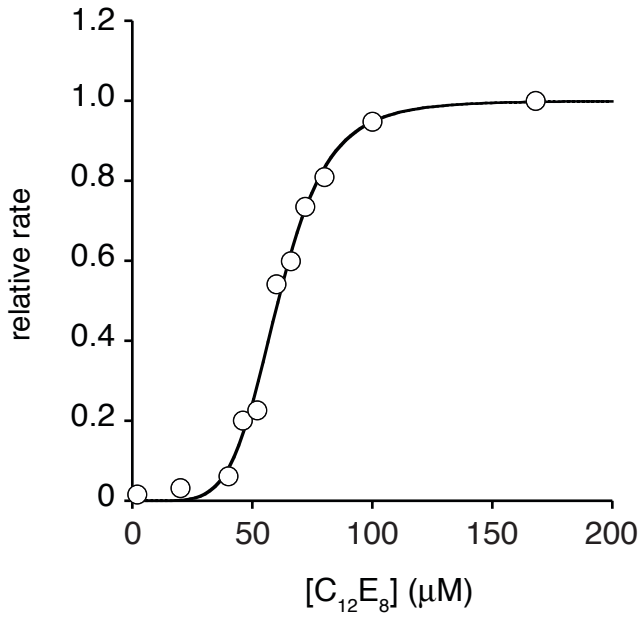

B

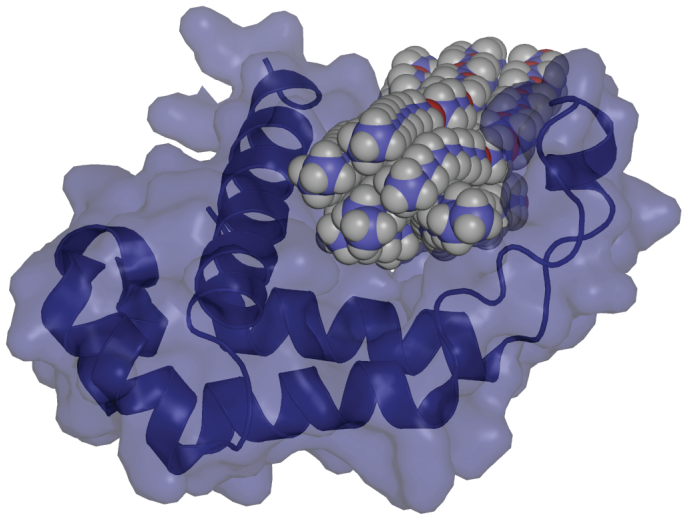

Figure S1

Figure S2. Addition of peptide does not induce aggregation of SRP under the assay conditions used. **A**. Binding of peptide to SRP is reversible. When peptide bound to 5 μM SRP is diluted 5 fold, the anisotropy returns to that seen for 1 μM SRP. Error bars represent the standard deviation of 3 independent measurements. **B**. Addition of 0.5 μM ΔEspP-FAM peptide to 50 μM SRP as used in anisotropy assays does not decrease the amount of Ffh still soluble after 1 hr. at 390,000 x *g*. **C**. No decrease in the fraction of soluble Ffh is observed upon addition of 10 μM ΔEspP* peptide to Ffh-FtsY binding reactions using 5 μM Ffh. Centrifugation is as per part B.

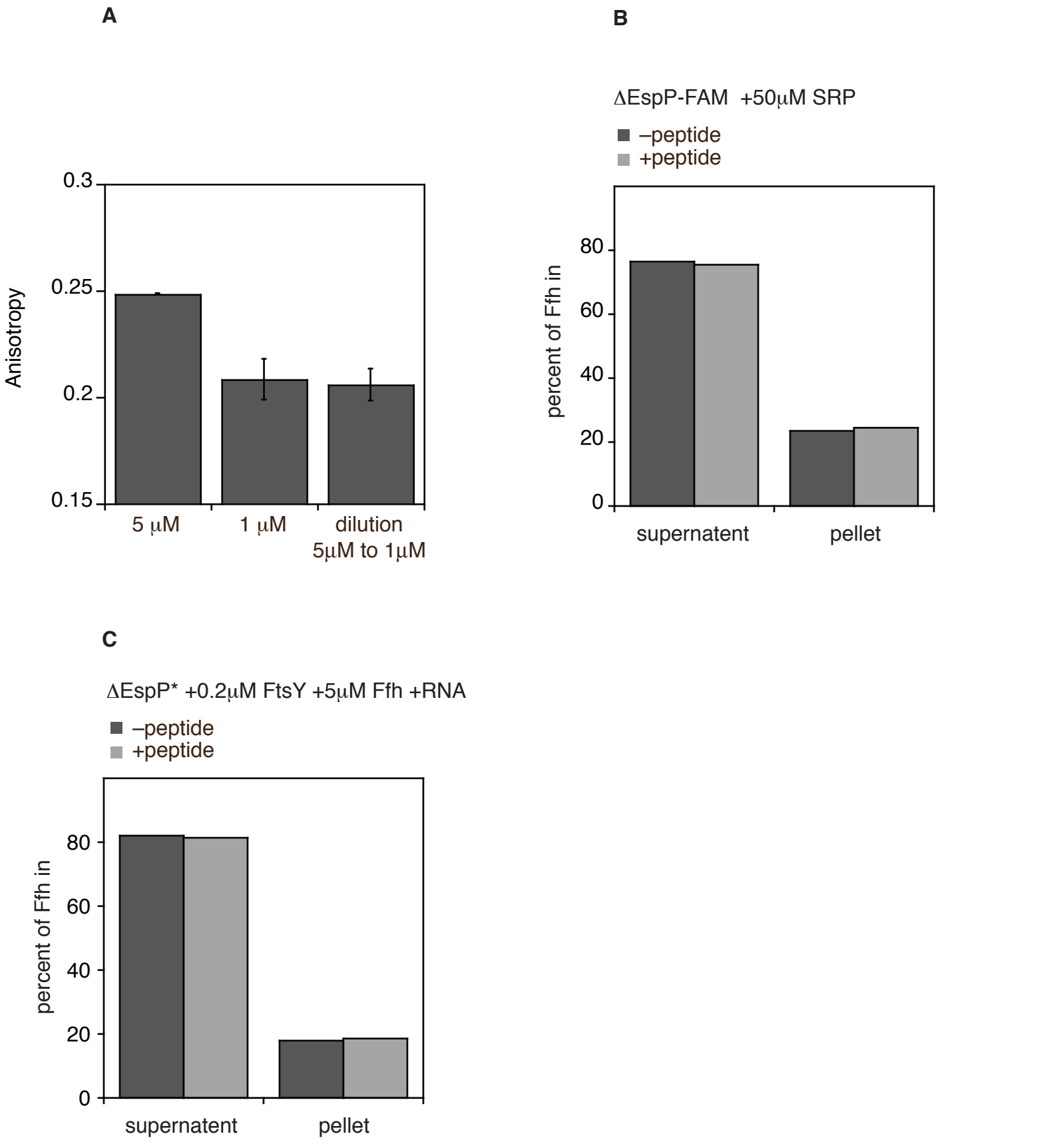
A
0.3
0.25
0.2
0.15
Anisotropy
5 μM
1 μM
dilution
5μM to 1μM
B
ΔEspP-FAM +50μM SRP
–peptide
+peptide
80
60
40
20
0
percent of Ffh in
supernatent
pellet
C
ΔEspP* +0.2μM FtsY +5μM Ffh +RNA
–peptide
+peptide
80
60
40
20
0
percent of Ffh in
supernatent
pellet

Figure S2

Figure S3. The GTP hydrolysis-driven disassembly of the Ffh•FtsY complex is insensitive to 4.5S RNA $C_{12}E_8$ and signal peptide. In addition to catalyzing Ffh•FtsY complex formation, 4.5S RNA stimulates the GTPase activity of the ^{GTP}Ffh-4.5S RNA•FtsY^{GTP} complex approximately 4-fold. To explore whether $C_{12}E_8$ and ΔEspP* also affect GTPase activity, we measured the rate of GTP hydrolysis-driven disassembly of ^{GTP}Ffh-4.5SRNA•FtsY^{GTP} complexes by a pulse chase procedure. ^{GTP}Ffh-4.5SRNA•FtsY^{GTP} complexes were formed and then rapidly mixed with an excess of GDP^{Mg++}. Complex disassembly was monitored by a decrease in tryptophan fluorescence. The disassembly rate is equal to the maximal rate of GTP hydrolysis by the ^{GTP}Ffh-4.5SRNA•FtsY^{GTP} complex. $C_{12}E_8$ and ΔEspP* had no effect on the maximal rate of GTP hydrolysis by the ^{GTP}Ffh-4.5SRNA•FtsY^{GTP} complex. Additionally, basal GTP hydrolysis was not affected by $C_{12}E_8$ (data not shown).

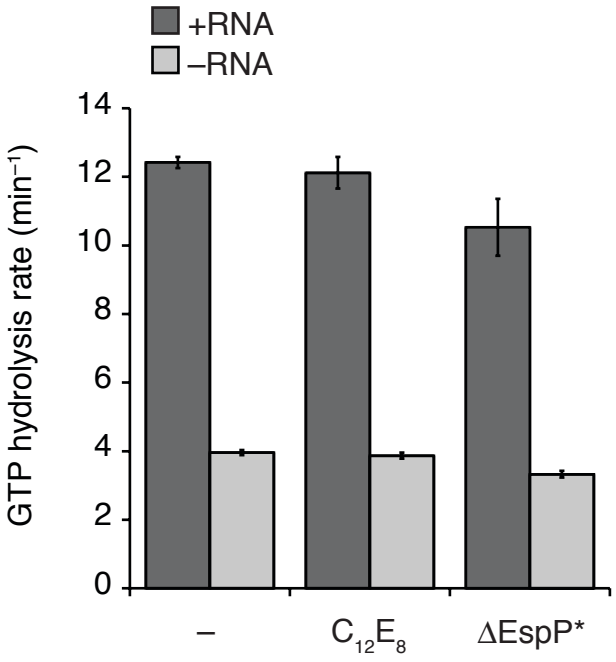

Figure S3

Figure S4. In figure 3, Ffh-4.5SRNA-FtsY binding assays were done at subsaturating concentrations (10 μM) of ΔEspP (F12A, L15T)* peptide (K_d 87 μM, figure 3A). Addition of increasing amounts of the ΔEspP (F12A, L15T)* peptide to 1μM FtsY with 2μM Ffh-4.5SRNA increased the k_{obs} for Ffh-4.5SRNA•FtsY complex formation.

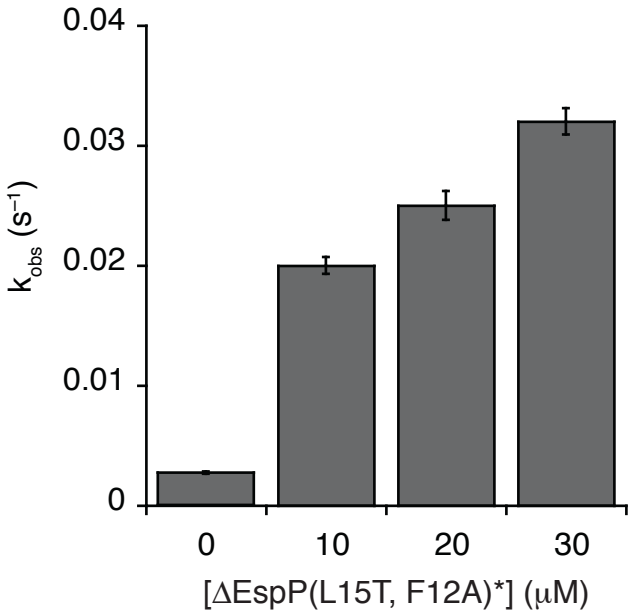

Figure S4

Figure S5. Model for the role of 4.5S RNA in cotranslational protein targeting. Signal peptides bind to the M-domain of Ffh as they emerge from ribosomes. Contact with signal peptide induces a conformational change in 4.5S RNA (Step 1), which activates the RNA. Activated 4.5S RNA communicates with the NG domain of Ffh (Step 2), priming it for interaction with FtsY by displacing the autoinhibitory helix α-N1 (Step 3). Encountering FtsY relaxes this transition state by displacing helix α-N1 of FtsY (Step 4), resulting in productive targeting of the ribosome nascent chain complex to the translocon. It is not known whether the displacement of helices N1 from Ffh and from FtsY occurs stepwise as depicted or in a concerted reaction only upon Ffh encountering FtsY. Next, the SRP/SR complex is disassembled by GTP hydrolysis to recycle the components for subsequent rounds of targeting.

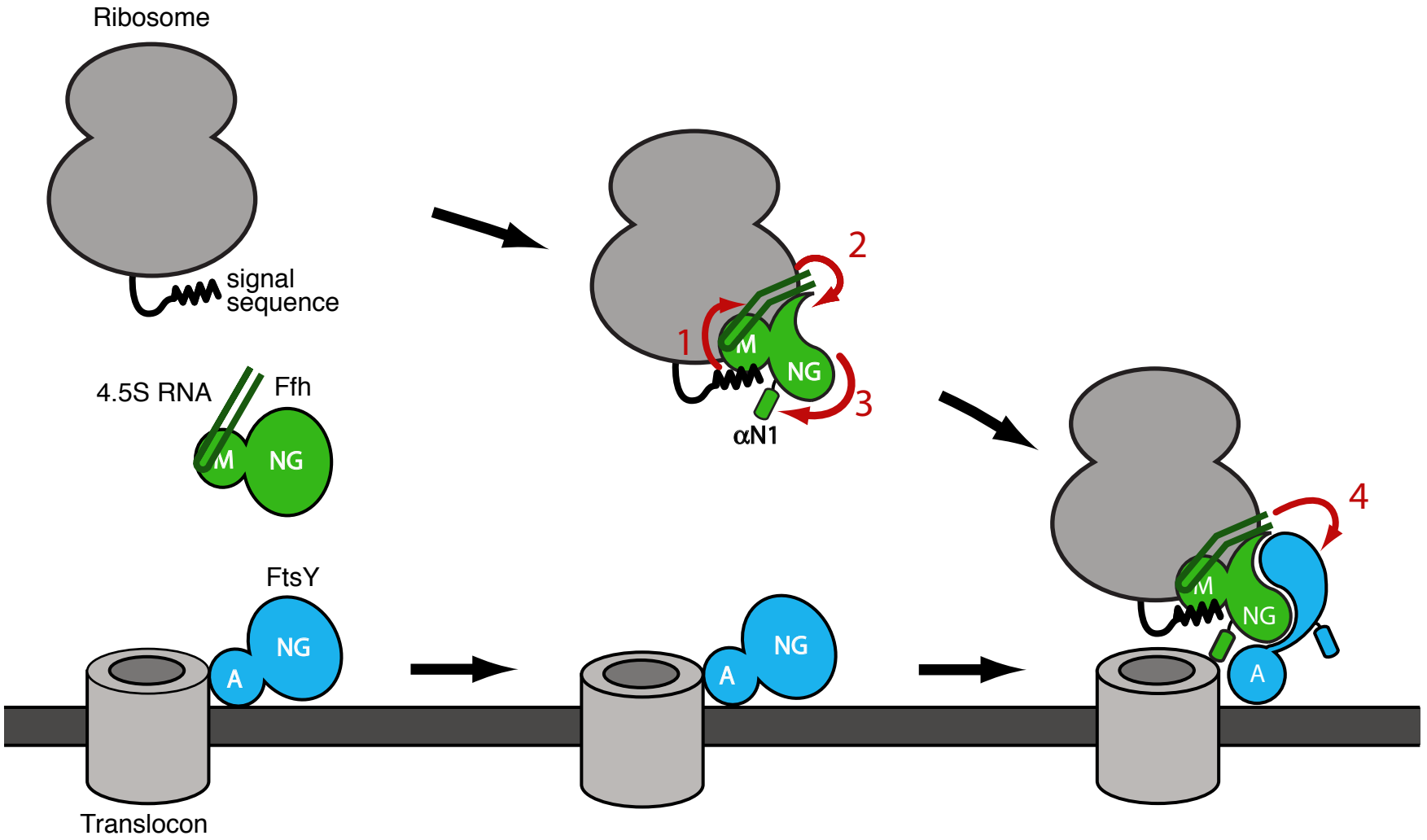
Ribosome
signal sequence
4.5S RNA
Ffh
M
NG
1
2
3
αN1
4
FtsY
NG
A
Translocon

Figure S5

Table and Legend.

Table S1: Association and dissociation rate constants for Ffh/FtsY association and dissociation. Rate constants were measured as described in methods in the presence or absence of detergent and peptides. In all cases, peptides were used at 10μM concentration and $C_{12}E_8$ was used at 185μM.

	k_{on} ($M^{-1}s^{-1}$)		k_{off} (s^{-1})	
RNA:	+	–	+	–
Additive:				
–	830 ± 50	110 ± 50	0.00010 ± 0.000003	0.0000056 ± 0.0000004
$C_{12}E_8$	60,000 ± 7000	140 ± 20	0.0023 ± 0.0001	0.0000089 ± 0.000001
ΔEspP*	36,000 ± 700	44 ± 20	0.0010 ± 0.00003	0.000014 ± 0.0000005
ΔEspP* + $C_{12}E_8$	83,000 ± 3000	N.D.	N.D	N.D
ΔEspP(F12A, L15T)*	7,000 ± 900	82 ± 10	0.00023 ± 0.000009	0.0000044 ± 0.0000005

References:

1. P. Peluso, S. O. Shan, S. Nock, D. Herschlag, P. Walter, *Biochemistry* **40**, 15224 (Dec 18, 2001).
2. M. Le Maire, S. Kwee, J. P. Andersen, J. V. Moller, *Eur J Biochem* **129**, 525 (Jan 1, 1983).
3. R. J. Keenan, D. M. Freymann, P. Walter, R. M. Stroud, *Cell* **94**, 181 (Jul 24, 1998).